Spectrum Management for Proactive Video Caching in Information-Centric Cognitive Radio Networks

Pengbo Si, *Senior Member, IEEE,* Hao Yue, *Member, IEEE,* Yanhua Zhang, and Yuguang Fang, *Fellow, IEEE*

***Abstract*—To deal with the rapid growth of mobile data traffic and the user interest shift from peer-to-peer communications to content dissemination based services such as video streaming, information-centric networking (ICN) has emerged as a promising architecture and has been increasingly used for wireless and mobile networks. In this paper, we focus on video dissemination in information-centric cognitive radio networks (IC-CRNs) and investigate the use of harvested bands for proactively caching video contents at the locations close to the interested users to improve the performance of video distribution. With consideration of the dynamic and unobservable nature of some parameters, we formulate the allocation of harvested bands as a Markov decision process with hidden and dynamic parameters, and transform it into a partially observable Markov decision process and a multi-armed bandit formulation. Based on them, we develop a new spectrum management mechanism which maximizes the benefit of proactive video caching as well as the efficiency of spectrum utilization in the IC-CRNs. Extensive simulation results demonstrate the significant performance improvement of the proposed scheme for video streaming.**

***Index Terms*—Video streaming, information-centric network, spectrum management, cognitive radio.**

I. Introduction

THE current Internet architecture has served as a global information infrastructure for several decades, which was primarily designed for meeting the communication demands between pairs of static hosts. However, it cannot accommodate the recent rapid growth of network traffic and the user interest shift from peer-to-peer communications to content dissemination based services, such as video streaming services where the users care about video contents themselves and are oblivious to the locations where the desired video resides. In this context, information-centric networking (ICN) has emerged as a promising candidate for the future Internet. ICN takes a novel information-centric communication model, where data is named, addressed and matched regardless of its location [1–4]. Each time a user intends to access a content item, it expresses its interest to the network. Then, the network will locate the best source of the desired content based on its name and deliver the content to the user. The ICN also favors the use of in-network caching [5, 6], which allows network devices to temporarily store the popular contents for users' future demand, to facilitate data access and retrieval. Therefore, content delivery delay can be further reduced and scalable content distribution can be efficiently achieved.

In recent years, with the popularity of mobile devices and various content dissemination based mobile services, the information-centric technologies have also been increasingly used in wireless networks [7]. In order to support the booming increase of wireless and mobile data traffic, especially the demand of video streaming from mobile devices such as tablets, smart phones, video game stations and augmented reality (AR) devices, traditional wireless networks inevitably face severe spectrum resource shortage. To address this problem, cognitive radio (CR) has been proposed to enable dynamic spectrum access from the unlicensed users, which have been recognized as an efficient method to improving the spectrum utilization and has attracted extensive attention from both academia and industries [8].

In this paper, we focus on video streaming in information-centric cognitive radio networks (IC-CRNs) with consideration of proactive video caching. Since it serves the future demand of users on video distribution, the traffic of proactive video caching is delay-tolerant in nature. Therefore, we can use the uncertain harvested bands in the CR networks (CRNs) to efficiently support the transmission of video contents for proactive caching, and save the reliable licensed bands for the real-time video streaming traffic, which could further increase spectrum efficiency in the IC-CRNs. In view of that, we propose a new spectrum management mechanism for IC-CRNs to dynamically allocate the harvested bands for proactive caching and optimize the performance of video distribution. In this mechanism, the proactive caching data with higher expected video quality improvement has the priority to utilize the harvested bands, and peak signal-to-noise ratio (PSNR) is adopted as the video quality criterion to calculate the expected video quality improvement. Even though some research efforts have been devoted to proactive caching and video streaming in ICNs [9–18], none of them concentrate on the use of harvested spectrum for proactive video caching in IC-CRNs. The main contributions of this paper are summarized as follows.

- We propose to use the uncertain low-cost harvested bands to transmit the delay-tolerant traffic for proactive video caching in IC-CRNs, which can improve the quality of video streaming services for mobile users as well as the

Manuscript received May 15, 2015. The work of P. Si and Y. Zhang was partially supported by the National Natural Science Foundation of China under Grants 61372089 and 61571021. The work of Y. Fang and H. Yue was partially supported by the US National Science Foundation under Grants CNS-1343356 and CNS-1409797. This work was completed while the first author was a Visiting Research Scholar with the Department of Electrical and Computer Engineering at University of Florida, Gainesville, FL, 32611 USA.

P. Si and Y. Zhang are with Beijing Advanced Innovation Center for Future Internet Technology, and the College of Electronic Information and Control Engineering, Beijing University of Technology, Beijing, 100124 China. E-mail: sipengbo@bjut.edu.cn and zhangyh@bjut.edu.cn.

H. Yue is with the Department of Computer Science, San Francisco State University, San Francisco, CA, 94132 USA. Email: haoyue@sfsu.edu.

Y. Fang is with the Department of Electrical and Computer Engineering, University of Florida, Gainesville, FL, 32611 USA. E-mail: fang@ece.ufl.edu.

spectrum utilization of the networks.

- Considering the dynamic and unobservable nature of some parameters in practice, we study the harvested spectrum allocation for video dissemination in IC-CRNs and formulate it as a Markov decision process with hidden and dynamic parameters,
- We reformulate the problem into a partially observable Markov decision process (POMDP) and a multi-armed bandit (MAB) problem, and design a new spectrum management mechanism to efficiently allocate the harvested bands and optimize the performance of proactive caching.
- We conduct extensive simulations and show the significant performance improvement of the proposed spectrum management scheme for video distribution over the existing methods.

The rest of this paper is organized as follows. The related work is presented in Section II. In Section III, we introduce the network architecture with proactive video caching. The system model is presented in Section IV and the spectrum management problem is formulated as an Markov decision process with hidden and dynamic parameters (HDP-MDP) in Section V. We solve the problem by POMDP and MAB reformulation in Section VI. Then, the process to allocate the bands and the complexity of solving the problem are discussed in Section VII. Extensive simulation results are presented and discussed in Section VIII and the conclusions are drawn in Section IX.

II. Related Work

In the literature, some research efforts have been devoted to proactive caching. Zhao et al. study the caching placement problem in multi-hop cognitive radio networks, aiming to minimize the caching cost with consideration of the data access delay [19]. Yu et al. propose an architecture to deploy ICN in wireless ad hoc networks, called ICAN, and discuss the push-based communications [9]. Considering the pushing operation in ICNs, a proactive content pushing scheme is proposed for content provider mobility support, which allows proactively pushing contents that are expected to be requested in the near future to proximity ICN routers [10]. Jung et al. propose a data push technique by using Interest Push Table (IPT) to support the push-based method required by some applications in the networks [11]. The bootstrap operation of a publish/subscribe information centric network is studied in [12], with the discussion on the content publishing process. In [13], a deployable and scalable information centric network architecture (DSINA) is introduced to handle user-generated content uploading and notification pushing.

To serve the future demand of users on video distribution, the information-centric architecture is widely accepted as a promising technique due to its capability of enabling efficient data delivery with in-network caching. The Internet Research Task Force (IRTF) started the Information-Centric Networking Research Group (ICNRG) in 2012 and are currently working on the adaptive video streaming over ICNs, among other ICN-related research issues [20]. An adaptive retransmission scheme is proposed in [14] to overcome video packet loss in content-centric wireless networks. A timeout estimation algorithm is also developed to adjust the timeout value. Han et al. propose a framework of adaptive mobile video streaming and sharing under the Named Data Networking (NDN) architecture [15]. In [16], MPEG dynamic adaptive streaming over HTTP (DASH) is implemented and evaluated in content-centric networking (CCN). The performance of in-network caching is analyzed in [17] based on the observation of rate adaptation of video streaming and cache-server oscillation in the ICN testbed. In [18], Tsilopoulos et al. compare the video services in two different ICN architectures, i.e., CCN and Publish-Subscribe Internetworking (PSI). In [21], the architecture of named data networking for cognitive radio ad hoc networks (NDN-CRAHNs) has been proposed, of which the main idea is introducing the concept of NDN into cognitive radio networks to maintain end-to-end quality-of-service. It shows that cognitive radio networks and information-centric networks could be jointly designed to form an effective future network architecture. Different from [21] and other works mentioned above, in our paper, ICN and CRNs are introduced to the future Internet to improve the performance of video streaming. Here, ICN is used to facilitate video access and dissemination via in-network caching, and CRNs can harvest additional spectrum resource to support the delay-tolerant video caching traffic and improve spectrum utilization for video streaming. Therefore, in our work, we consider both ICN and CRNs, and design a new spectrum allocation mechanism to maximize the benefit of video caching for video streaming as well as optimize the video quality at end users.

III. Information-Centric Cognitive Radio Networks

In this section, we describe the network architecture as well as the proactive video caching operations.

A. Network Architecture

We have proposed a new architecture for CRNs in [22–24], which consists of a secondary service provider (SSP), base stations, CR routers and mobile users. There are two types of spectrum bands in the network: the basic bands, which are reserved for the network, and the harvested bands, which are harvested from the primary network. A collection of CR routers are deployed in the network to facilitate wireless access for mobile users. The CR routers also cooperatively sense the primary network's spectrum bands and report the sensing results to the SSP. Based on the sensing results, the SSP collectively harvests the vacant licensed spectrum resources from the primary network, and allocates both the basic bands and the harvested bands to the CR routers for data transmission. In this paper, we introduce the information-centric networking technology into this architecture, and the resulted IC-CRN is shown in Fig. 1. The CR routers are upgraded with embedded cache, which are called CCRs in the rest of the paper, for temporarily storing the video contents that users are interested in. The CCRs are also capable of transmitting or receiving multiple packets simultaneously over multiple bands, with each packet transmitted over each band.

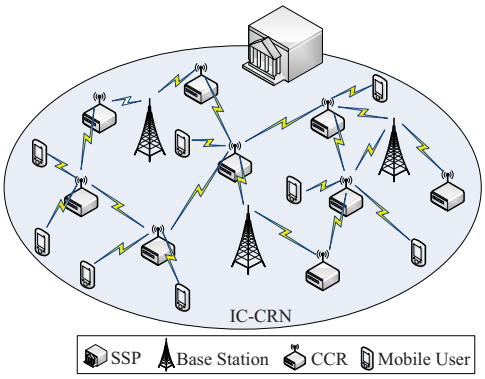

Fig. 1: IC-CRN architecture.

Moreover, we adopt the asynchronous packet transmission mode to improve the spectrum utilization efficiency. Different from the synchronous mode in which fixed-length time slots are used as the unit for band allocation and data transmission, the asynchronous mode allows the SSP to allocate a band to a CCR whenever the band is available, and the CCR could utilize the band immediately after the allocation.

B. Proactive Video Caching

In this work, we consider proactive video caching in the IC-CRNs, where some popular video contents are cached at the CCRs close to the interested users in order to reduce the delivery latency for their future demand. In practice, due to the fact that the caching capacity is always limited, a CCR should replace the out-of-date content with new and popular video segments, even if the segments are currently cached at another CCR and no user is requesting it. For example, compared to a video segment *A* that resides at CCR-1, another segment *B* currently in CCR-2 could achieve higher expected PSNR improvement if it is cached at CCR-1. Thus, *B* will be proactively pushed from CCR-2 to CCR-1 to replace *A*. An information-centric routing algorithm is adopted for proactive video caching delivery in a distributed manner as in [25].

In IC-CRNs, the uncertain but low-cost harvested bands are suitable to transmit the proactive caching video (CaV) traffic due to its delay-tolerant nature. The regular video streaming (ReV) traffic is delay-sensitive, and therefore, should mainly reply on the basic bands of the IC-CRN to transmit[1]. In case of low ReV traffic in both primary and IC-CRNs, e.g., during nighttime, a large number of harvested bands could be efficiently utilized for proactive CaV data transmissions.

IV. System Model

The network, service, video quality and in-network caching models are presented in this section.

A. Network Model

We consider an IC-CRN with a collection of CCRs and mobile users. Let $\mathbb{Z}$ denote the set of CCRs, and Z denote the size of $\mathbb{Z}$, i.e., $Z = |\mathbb{Z}|$. We use t to represent the time instance, where $t \geq 0$. Here, infinite time length is considered. Let C denote the total number of spectrum bands that can be harvested by the IC-CRN, and $\mathbb{C}_t$ denote the set of harvested bands used for proactive caching at time t. The availability of the harvested bands for proactive caching can be modeled as a Poisson process, with the harvesting rate λ_{H}. Thus, the probability density function of the inter-arrival time τ_{H} can be represented as $f(\tau_{\mathrm{H}}) = \lambda_{\mathrm{H}} e^{-\lambda_{\mathrm{H}}\tau_{\mathrm{H}}}$. In practice, the values of λ_{H} may change over time due to the traffic dynamics in both the primary network and the IC-CRN. In this paper, we only consider two time periods for simplicity, i.e., busy time and idle time, and use $\lambda_{\mathrm{H},1}$ and $\lambda_{\mathrm{H},2}$ to denote the value of λ_{H} during the busy time and idle time, respectively. However, our work can be easily extended to the case with more levels of λ_{H}.

The achievable video bit rate for a mobile user depends on the rate of the bottleneck link along the transmission path of the video. Let ω_y denote the random bit rate of the link y, with the cumulative distribution function $F_{\Omega_y}(\omega_y)$. Assume ω_y at different links are independent. Then, the achievable bit rate $\omega_{\mathrm{A}}(z_{\mathrm{S}}, z_{\mathrm{D}})$ from the source CCR z_{S} to the destination CCR z_{D} where the mobile user is directly connected can be represented as

$$\omega_{\mathrm{A}}(z_{\mathrm{S}}, z_{\mathrm{D}}) = \min_{y \in \mathbb{Y}(z_{\mathrm{S}}, z_{\mathrm{D}})} \omega_y, \tag{1}$$

where $\mathbb{Y}(z_{\mathrm{S}}, z_{\mathrm{D}})$ is the set of links along the path from z_{S} to z_{D}. We set $\omega_{\mathrm{A}}(z_{\mathrm{D}}, z_{\mathrm{D}}) = \infty$ to denote the case where the video is streamed from the CCR directly connected to the user. Then, if $z_{\mathrm{S}} \neq z_{\mathrm{D}}$, the cumulative distribution function of $\omega_{\mathrm{A}}(z_{\mathrm{S}}, z_{\mathrm{D}})$ is represented as

$$F_{\Omega_{\mathrm{A}}(z_{\mathrm{S}}, z_{\mathrm{D}})}(\omega) = \sum_{y \in \mathbb{Y}} \left\{ F_{\Omega_y}(\omega) \prod_{y' \in \mathbb{Y}, y' \neq y} \left[1 - F_{\Omega_{y'}}(\omega) \right] \right\}. \tag{2}$$

B. Service Model

As mentioned above, we consider two types of traffic in IC-CRNs: ReV traffic and CaV traffic, which carry the data for regular video streaming and the data for proactive video caching, respectively. Since delay-sensitive ReV packets have higher priority than delay-tolerant CaV packets, all ReV packets are placed ahead of all CaV packets in the transmission queue of a CCR. Let $\mathbb{Z}_{\mathrm{ReV}}(t)$ and $\mathbb{Z}_{\mathrm{CaV}}(t)$ denote the sets of CCRs whose first packets to transmit are ReV and CaV packets at time t, respectively. We also use $\mathbb{Z}_{\mathrm{null}}(t)$ to represent the set of CCRs whose transmission queues are empty at time t. Obviously, we have $\mathbb{Z}_{\mathrm{ReV}}(t) \cap \mathbb{Z}_{\mathrm{CaV}}(t) = \mathbb{Z}_{\mathrm{ReV}}(t) \cap \mathbb{Z}_{\mathrm{null}}(t) = \mathbb{Z}_{\mathrm{null}}(t) \cap \mathbb{Z}_{\mathrm{CaV}}(t) = \Phi$, and $\mathbb{Z}_{\mathrm{ReV}}(t) \cup \mathbb{Z}_{\mathrm{CaV}}(t) \cup \mathbb{Z}_{\mathrm{null}}(t) = \mathbb{Z}$.

Each CaV packet π contains a video segment d_π. Let $z_{\mathrm{S}}(\pi)$ and $z_{\mathrm{D}}(\pi)$ denote the source and destination CCRs of π, respectively. Let $z_{\mathrm{C}}(\pi, t)$ be the CCRs at π is at time t. Moreover, $\xi(\pi) = |\mathbb{Y}(z_{\mathrm{S}}(\pi), z_{\mathrm{D}}(\pi))|$ is used to represent the number of hops from $z_{\mathrm{S}}(\pi)$ to $z_{\mathrm{D}}(\pi)$. The arrival of CaV packets at a CCR z is modeled as a Poisson process, with the CaV packet arriving rate λ_z.

[1]ReV traffic may also use harvested bands if the basic bands cannot satisfy its requirement.

C. Video Quality Model

Rate control mechanisms are widely adopted in recent advanced video coding algorithms such as H.264 and MPEG-4, in which the intra-refreshing rate of macroblocks is used to control the video encoder output bit rate and the error resilience mechanism for error protection. Given a data rate for a video streaming, a rate-distortion (R-D) model is studied in [26, 27] for H.264/AVC video coding with rate control. Let $\omega_{\max}$ denote the source coding rate of the video. Then, the video bit rate can be represented as

$$\omega = \min\left[\omega_{\max}, \omega_{\mathrm{A}}(z_{\mathrm{S}}, z_{\mathrm{D}})\right]. \tag{3}$$

and the cumulative distribution function of ω is

$$F_{\Omega}(\omega) = \begin{cases} F_{\Omega_{\mathrm{A}}}(\omega_{\mathrm{A}}), & \text{if } \omega < \omega_{\max}, \\ 1, & \text{otherwise.} \end{cases} \tag{4}$$

We adopt the video PSNR to evaluate the video quality. Let $\rho(\omega)$ denote the PSNR when the video streaming bit rate is ω. In this paper, we consider the average PSNR $\bar{\rho}(\omega)$, which can be calculated as follows:

$$\bar{\rho}(\omega) = \int_0^{\infty} \rho(\omega) \mathrm{d}F_{\Omega}(\omega). \tag{5}$$

According to Eqn. (3), when $\omega_{\max}$ is determined, the video bit rate ω only depends on the source CCR z_{S} and the destination CCR z_{D}. Therefore, we use $\bar{\rho}(z_{\mathrm{S}}, z_{\mathrm{D}})$ instead of $\bar{\rho}(\omega)$ in the rest of the paper.

D. In-Network Caching Model

In information-centric networks, the hit ratio is a common criterion for in-network cache management [28]. Here, the hit ratio is defined as the ratio between the number of cache hits and the total requests observed over a period of time. Higher hit ratio indicates more user requested video contents can be delivered from the nearby CCRs, so that better video quality could be achieved.

The hit ratio of a cached video segment depends on user interests and the distribution of users in the network. A user would benefit from in-network caching more significantly if the video be interested are cached at the CCR directly connected to it. Thus, we only consider hits of a cached video segment from directly-connected users for simplicity, and denote $b(z, d_\pi, t)$ as the expected hit ratio of a video segment d_π at time t by the users directly connected to CCR z.

During the delivery of a CaV packet π from $z_{\mathrm{S}}(\pi)$ to $z_{\mathrm{D}}(\pi)$, the video segment d_π may be cached at $z_{\mathrm{D}}(\pi)$ via regular video transmissions. In this case, proactive caching for d_π will not contribute to the PSNR improvement. Thus, π will be removed from the transmission queue.

V. Problem Formulation

In this section, the spectrum management problem is formulated as a Markov decision process with hidden and dynamic parameters.

A. System State Space

The state of the whole system is a combination of the substates of all CCRs. To characterize the benefit provided by proactive caching of the video contents at the CCRs close to the users, we define the expected reward $\tilde{\beta}(z,t)$ in Eqn. (6) as the expected PSNR improvement by transmitting the first CaV packet π in the transmission queue at z to the next hop if π can be successfully delivered to $z_{\mathrm{D}}(\pi)$. Here, $d^*(z_{\mathrm{D}}(\pi), t)$ is the video segment with the lowest expected video quality improvement among all segments cached at $z_{\mathrm{D}}(\pi)$ at t, and $z_{\mathrm{S}}(d^*(z_{\mathrm{D}}(\pi), t))$ is the original server that publishes $d^*(z_{\mathrm{D}}(\pi), t)$. Note that given the CCR z and the time t, the first CaV packet π is known. Consequently, we use $\tilde{\beta}(z,t)$ in Eqn. (6) to indicate that the expected PSNR improvement depends on z and t only. The first part in the brace in Eqn. (6) denotes the expected PSNR improvement by caching d_π at $z_{\mathrm{D}}(\pi)$, and the second part represents the expected PSNR improvement by caching the segment $d^*(z_{\mathrm{D}}(\pi))$ which will be replaced by d_π. Besides, let d_0 denote a virtual segment which does not actually exist, to represent the case that the video segment caching space is vacant. Thus, $b(z_{\mathrm{D}}(\pi), y, d^*(z_{\mathrm{D}}(\pi), t), t) = 0$ should be adopted due to the fact that the hit ratio of a vacant caching space is zero. In this case, the destination CCR has available caching space for the new segment d_π, and no existing cached segment has to be replaced by d_π.

If π arrives at the destination $z_{\mathrm{D}}(\pi)$ successfully, $\xi(\pi)\tilde{\beta}(z,t)$ can be obtained, indicating the expected PSNR improvement to replace $d^*(z_{\mathrm{D}})$ by d_π. However, if π fails to arrive at $z_{\mathrm{D}}(\pi)$ because d_π has been cached at $z_{\mathrm{D}}(\pi)$ before π arrives at $z_{\mathrm{D}}(\pi)$, the reward for delivering π should be zero. We define the cached-in-destination indicator $\delta(\pi, t)$ as

$$\delta(\pi, t) = \begin{cases} 1, & \text{if } \pi \text{ is cached in } z_{\mathrm{D}}(\pi) \text{ at } t, \\ 0, & \text{otherwise.} \end{cases} \tag{7}$$

The probability that $\delta(\pi, t)$ transits from 0 to 1 in one hop is denoted as P'_δ. Then, considering both the cases that π is successful delivered and π is discarded during delivery, the expected PSNR improvement by transmitting the first CaV packet π in the transmission queue at z to the next hop can be represented as $\tilde{\beta}'(z,t) = (1 - P'_\delta)^{\xi'(\pi)}\,\tilde{\beta}(z,t)$, where $\xi'(\pi)$ is the number of hops for which π still needs to be delivered to its destination $z_{\mathrm{D}}(\pi)$ after z.

We use discrete reward $\beta(z,t)$ instead of the continuous $\tilde{\beta}'(z,t)$. Let $S_{\beta-1}$ denote the number of levels of $\beta(z,t)$, and ϵ_m, $1 \le m \le S_\beta - 1$, denote the boundary values between two adjacent levels. Then,

$$\beta(z,t) = \begin{cases} \dot{\beta}_0, & \text{if } \tilde{\beta}(z,t) < \epsilon_1, \\ \dot{\beta}_m, & \text{if } \epsilon_m \le \tilde{\beta}(z,t) < \epsilon_{m+1}, \\ \dot{\beta}_{S_\beta - 1}, & \text{if } \tilde{\beta}(z,t) \ge \epsilon_{S_\beta - 1}, \end{cases} \tag{8}$$

where $\dot{\beta}_m$, $0 \le m \le S_\beta - 1$, are the realizations of $\beta(z,t)$. Obviously, $\dot{\beta}_m < \dot{\beta}_{m'}$ if $m < m'$. Let $\epsilon_1 = 0$, so that $\beta(z,t) = \dot{\beta}_0$ happens only when no CaV packet is in the queue.

The system state can be denoted as $s(t) = [\beta(z,t)]_{z\in\mathbb{Z}}$. Let $\mathbb{S}$ be the state space of $s(t)$. Then, $\mathbb{S} = \underbrace{\mathbb{S}_\beta \times \cdots \times \mathbb{S}_\beta}_{Z}$,

$$\tilde{\beta}(z,t) = \frac{1}{\xi(\pi)}\{b(z_{\rm D}(\pi),d_\pi,t)\left[\bar{\rho}(z_{\rm D}(\pi),z_{\rm D}(\pi))-\bar{\rho}(z_{\rm S}(\pi),z_{\rm D}(\pi))\right] -b(z_{\rm D}(\pi),y,d^*(z_{\rm D}(\pi),t),t)\left[\bar{\rho}(z_{\rm D}(\pi),z_{\rm D}(\pi))-\bar{\rho}(z_{\rm S}(d^*(z_{\rm D}(\pi),t)),z_{\rm D}(\pi))\right]\}. \quad (6)$$

where $\mathbb{S}_\beta$ is the state space of $\beta(z,t)$. The size of $\mathbb{S}$ can be represented as $|\mathbb{S}| = |\mathbb{S}_\beta|^Z = {S_\beta}^Z$.

B. Actions and Policies

Whenever the IC-CRN harvests a new available spectrum band, the band allocation decision is made by the SSP according to the current system state $s(t)$. Let $a(t)$ represent the decision made at t, and $\mathbb{A}$ represent the set of all available actions. At each time instance t, only one band is allocated to one of the CCRs[2]. Then, $a(t)$ can be represented as $a(t)=z$ if the new harvested band is allocated to z at t.

We define the action of z as

$$a_z = \begin{cases} 0, & \text{if } a(t_k)\neq z,\\ 1, & \text{if } a(t_k)=z. \end{cases} \quad (9)$$

Let t_k represent the kth decision time instance. Actions $a(t_k)$ executed at all decision time instances t_k form a policy l for the system, i.e., $l=\{a(t_0),a(t_1),\ldots,a(t_k),\ldots\}$. Let $\mathbb{L}$ denote the set of all available policies. An optimal policy l^* is the policy that achieves the maximum system reward, which will be discussed in Section V-D.

C. State Transitions

We first define $\kappa(z,t)$ as the no-CaV-packet indicator.

$$\kappa(z,t) = \begin{cases} 1, \text{if no CaV packet is in } z\text{'s transmission queue at } t,\\ 0, \text{otherwise.} \end{cases} \quad (10)$$

To derive the system state transition probability, we define the following probabilities.

$P_{\rm V}(v,\lambda_{\rm H},\lambda_z)$: The average probability that v CaV packets arrive during two adjacent decision time instances.

P_δ: The probability that $\delta(\pi,t_k)=0$ transits to $\delta(\pi,t_{k+1})=1$ between two decision time instances, i.e., $P_\delta = {\rm P}\left(\delta(\pi,t_{k+1})=1|\delta(\pi,t_k)=0\right)$.

$P_\kappa(z)$: The probability that no CaV Packet is in the queue at t_k and a CaV packet arrives for transmission during $t_k<t<t_{k+1}$, i.e., $P_\kappa(z)={\rm P}\left(\kappa(z,t_{k+1})=0|\kappa(z,t_k)=1\right)$.

$P_{\dot{\beta}_{z,j}}$: The probability that the next packet is in the state $\dot{\beta}_{z,j}$, for $\dot{\beta}_{z,j}\in\mathbb{S}_\beta$.

$P^*_{\dot{\beta}_{z,j}}$: The probability that $\beta(z,t)=\dot{\beta}_{z,j}$ among $\dot{\beta}_{z,j}\in\mathbb{S}_\beta, \dot{\beta}_{z,j}\neq\dot{\beta}_0$. Thus, we have $P^*_{\dot{\beta}_{z,j}} = P_{\dot{\beta}_{z,j}}/\sum_{\dot{\beta}_{z,j}\in\mathbb{S}_\beta,\dot{\beta}_{z,j}\neq\dot{\beta}_0}P_{\dot{\beta}_{z,j}}$, for $\dot{\beta}_{z,j}\neq\dot{\beta}_0$.

$P^0_z(i,j)$: The one-step transition probability of $\beta(z,t)$ from $\dot{\beta}_{z,i}$ to $\dot{\beta}_{z,j}$ under action $a(t_k)\neq z$.

$P^1_z(i,j)$: The one-step transition probability of $\beta(z,t)$ from $\dot{\beta}_{z,i}$ to $\dot{\beta}_{z,j}$ under action $a(t_k)=z$.

[2]If multiple harvested bands are available simultaneously, they will be allocated one-by-one, at different time instances.

$P^a_s(i,j)$: The one-step transition probability of $s(t)$ from $\dot{s}_i$ to $\dot{s}_j$ under action $a(t_k)=\dot{a}_i$.

Then, we can have the following lemmas.

Lemma 1. $P_\kappa(z)=1-\frac{\lambda_H}{\lambda_z+\lambda_H}$.

Proof. Available in Section 1 in our proofs of the lemmas and theorems [29]. □

Lemma 2. *The random process $\beta(z,t)$ is a Markov decision process, of which the one-step transition probability is*

$$P^0_z(i,j) = \begin{cases} 1-P_\kappa(z), & \text{if } \dot{\beta}_{z,j}=\dot{\beta}_{z,i}=\dot{\beta}_0,\\ P_\kappa(z)P^*_{\dot{\beta}_{z,j}}, & \text{if } \dot{\beta}_{z,j}\neq\dot{\beta}_{z,i},\dot{\beta}_{z,i}=\dot{\beta}_0,\\ 1-P_\delta+P_\delta P_{\dot{\beta}_{z,i}}, & \text{if } \dot{\beta}_{z,j}=\dot{\beta}_{z,i}\neq\dot{\beta}_0,\\ P_\delta P_{\dot{\beta}_{z,j}}, & \text{if } \dot{\beta}_{z,j}\neq\dot{\beta}_{z,i},\dot{\beta}_{z,i}\neq\dot{\beta}_0, \end{cases} \quad (11)$$

and

$$P^1_z(i,j) = \begin{cases} 1-P_\kappa(z), & \text{if } \dot{\beta}_{z,j}=\dot{\beta}_{z,i}=\dot{\beta}_0,\\ P_\kappa(z)P^*_{\dot{\beta}_{z,j}}, & \text{if } \dot{\beta}_{z,j}\neq\dot{\beta}_{z,i},\dot{\beta}_{z,i}=\dot{\beta}_0,\\ P_{\dot{\beta}_{z,j}}, & \text{if } \dot{\beta}_{z,i}\neq\dot{\beta}_0. \end{cases} \quad (12)$$

Proof. Available in Section 2 in our proofs of the lemmas and theorems [29]. □

Furthermore, the transition probability of $s(t)$ can be derived as shown in the following theorem.

Theorem 1. *The random process $s(t)$ is a Markov decision process, of which the one-step transition probability is $P^a_s(i,j)=\prod_{z\in\mathbb{Z}}P^{a_z}_z(i,j)$.*

Proof. Available in Section 3 in our proofs of the lemmas and theorems [29]. □

We use $\mathbf{P}^a=[P^a_s(i,j)]$ to represent the one-step transition probability matrix of the system state $s(t)$ under action $a(t)$. In the one-step transition probabilities derived above, λ_z is a constant that can be estimated by observing the CaV packet arriving at z. However, it is non-trivial to derive or observe the probabilities ${\rm P}_\delta$ and ${\rm P}^*_{\dot{\beta}_{z,j}}$. Moreover, $\lambda_{\rm H}$ may change over time, due to the dynamics of the traffic load in both the primary network and the IC-CRN.

D. Objective and Reward

Proactive video caching aims to maximize the expected video PSNR at the mobile users. Therefore, $\beta(z,t_k)$ is obtained as the reward if a band is allocated to the CCR z, and no reward is obtained if no band is allocated to z. That is,

$$R_z(t_k) = \begin{cases} \beta(z,t_k), & \text{if } a(t)=z,\\ 0, & \text{otherwise.} \end{cases} \quad (13)$$

The total immediate reward at t_k can be represented as $R(t_k)=\sum_{z\in\mathbb{Z}}R_z(t_k)$, and our optimization problem can be represented as $l^*=\underset{l\in\mathbb{L}}{\rm argmax}\,R_{\rm ave}$, where

R_{ave} is the average long-term total reward, $R_{\text{ave}} = \lim_{K\to\infty} \frac{1}{K} \sum_{k=1}^{K} \gamma^{K-k} R(t_k)$. Here, γ is the discount factor, $0 < \gamma < 1$, and K is the number of decision time instances considered.

VI. Solving the HDP-MDP problem

In the previous section, the spectrum management problem is formulated as a Markov decision process (MDP). However, existing algorithms of MDPs cannot be directly applied to solve it because of the dynamic parameter λ_{H} and the unknown parameters P_δ and $\text{P}^*_{\dot{\beta}_{z,j}}$. To address this problem, we reformulate it as an augmented POMDP. Furthermore, an MAB formulation is introduced to reduce computational complexity of this problem.

A. Hidden Markov Decision Process Reformulation

Different values of λ_{H}, i.e., $\lambda_{\text{H},1}$ and $\lambda_{\text{H},2}$, are considered as different modes in this problem. These modes have distinct environment dynamics and require different control policies [30]. We need to learn its actual value while making the optimal spectrum allocation decisions. Suppose the expected durations of busy time and idle time are $\bar{\tau}_1$ and $\bar{\tau}_2$, respectively. Then, the mode transition probability matrix is represented as

$$\mathbf{P}_{\text{H}} = \begin{bmatrix} P_{\text{H}}(1,1) & P_{\text{H}}(1,2) \\ P_{\text{H}}(2,1) & P_{\text{H}}(2,2) \end{bmatrix}, \tag{14}$$

where

$$\begin{aligned} P_{\text{H}}(1,1) &= 1 - \frac{1}{\lambda_{\text{H},1}\bar{\tau}_1}, P_{\text{H}}(1,2) = \frac{1}{\lambda_{\text{H},1}\bar{\tau}_1}, \\ P_{\text{H}}(2,1) &= \frac{1}{\lambda_{\text{H},2}\bar{\tau}_2}, P_{\text{H}}(2,2) = 1 - \frac{1}{\lambda_{\text{H},2}\bar{\tau}_2}. \end{aligned} \tag{15}$$

The hidden-mode MDP formulated in Section V can then be converted into a POMDP by the transformations in [30]. We use the tuple $\langle \mathbb{S}', \mathbb{A}', \mathbf{P}', R', \mathbb{O}', \mathbf{Q}' \rangle$ to denote the state space, action space, state transition probability matrix, reward function, observation space and observation probability matrix of the resulting POMDP. Let the mode space of λ_{H} be $\mathbb{H}$. Then, $\mathbb{S}'$, $\mathbb{A}'$, $\mathbf{P}'$, R', $\mathbb{O}'$ and $\mathbf{Q}'$ can be derived based on $\mathbb{S}$, $\mathbb{A}$, $\mathbf{P}$, R and $\mathbb{H}$ as follows.

$$\begin{aligned} \mathbb{S}' &= \mathbb{S} \times \mathbb{H}, \\ \mathbb{A}' &= \mathbb{A}, \\ \mathbf{P}' &= [P'^a_s(i,j)] = \begin{bmatrix} \text{P}_{\text{H}}(1,1)\mathbf{P}^a & \text{P}_{\text{H}}(1,2)\mathbf{P}^a \\ \text{P}_{\text{H}}(2,1)\mathbf{P}^a & \text{P}_{\text{H}}(2,2)\mathbf{P}^a \end{bmatrix}, \\ R' &= R, \\ \mathbb{O}' &= \mathbb{S}, \\ \mathbf{Q}' &= [\text{P}(o(t) = \dot{o}_j | s(t) = \dot{s}_i)] = \begin{bmatrix} \mathbf{I}_S \\ \mathbf{I}_S \end{bmatrix}, \end{aligned} \tag{16}$$

where $\mathbf{P}^a$ is the state transition probability matrix whose elements are $P^a_s(i,j)$, $\text{P}(o(t) = \dot{o}_j | s(t) = \dot{s}_i)$ is the probability that the realization of the state is $\dot{s}_i$ with the observation $\dot{o}_j$, and $\mathbf{I}_S$ is an identity matrix of size $S = |\mathbb{S}|$.

B. Augmented POMDP Reformulation

To deal with the unknown parameters P_δ and $\text{P}^*_{\dot{\beta}_{z,j}}$, we further reformulate the HDP-MDP problem as an augmented POMDP, which is represented as a tuple $\langle \mathbb{S}'', \mathbb{A}'', \mathbf{P}'', R'', \mathbb{O}'', \mathbf{Q}'' \rangle$. Here, the action space $\mathbb{A}''$, reward R'', observation space $\mathbb{O}''$ and observation probability matrix $\mathbf{Q}''$ remain unchanged, i.e., $\mathbb{A}'' = \mathbb{A}'$, $R'' = R'$, $\mathbb{O}'' = \mathbb{O}'$, and $\mathbf{Q}'' = \mathbf{Q}'$.

To compute the state space, we need to use the similar method as in Eqn. (8) to obtain the discrete forms of P_δ and $P^*_{\dot{\beta}_{z,j}}$, which are denoted as $\hat{P}_\delta$ and $\hat{P}^*_{\dot{\beta}_{z,j}}$, respectively. Their value spaces are $\mathbb{W}_\delta$ and $\mathbb{W}^*_{\dot{\beta}_{z,j}}$, with the sizes $|\mathbb{W}_\delta| = W_\delta$ and $\left|\mathbb{W}^*_{\dot{\beta}_{z,j}}\right| = W^*_{\dot{\beta}_{z,j}}$, respectively. Then, the unknown parameter space $\mathbb{W} = \mathbb{W}_\delta \times \left(\mathbb{W}^*_{\dot{\beta}_{z,j}}\right)^Z$. Given the POMDP state space $\mathbb{S}'$ and the parameter space $\mathbb{W}$, the augmented state space can be represented as $\mathbb{S}'' = \mathbb{S}' \times \mathbb{W}$ [31]. Moreover, the element in the ith row and jth column of the transition probability matrix $\mathbf{P}''$ is computed according to Eqn. (17), where $s''(t_k)$ and $s''(t_{k+1})$ are states of the augmented POMDP, $s'(t_k)$ and $s'(t_{k+1})$ are states of the original POMDP, $w(t_k)$ and $w(t_{k+1})$ are the states of the unknown parameters, $w(t_k)$ and $w(t_{k+1}) \in \mathbb{W}$, and $\eta(\dot{w}_i, \dot{w}_j)$ is the Kronecker delta function that $\eta(\dot{w}_i, \dot{w}_j) = 1$ if $\dot{w}_i = \dot{w}_j$, and $\eta(\dot{w}_i, \dot{w}_j) = 0$ otherwise.

After we obtain the augmented POMDP formulation, the off-line POMDP planning can be performed and this augmented POMDP problem can be solved to obtain an optimal or near-optimal policy. The off-line computation needs to be operated only once during network initialization. Then, the results can be stored locally for future use, and no further high-complexity computation is necessary even if the network is shut down and restarted. The only case that we need to run the off-line computation again is when the settings of the network are changed. The computational complexity of the on-line process is low and thus real-time processing can be achieved. Existing solutions can also balance exploration and exploitation by searching in the space of beliefs and optimizing the expected total reward [32].

C. MAB Reformulation

To solve the previously formulated POMDP problem, the SSP needs to collect the state information of all CCRs and make globally-optimal decisions. Since the state space is large, the computational complexity for the SSP to solve this problem is significantly high (detailed problem size analysis will be presented in Section VII-B and VII-C). In this subsection, we introduce the multi-armed bandit formulation to enable distributed optimization and improve the computational efficiency of this problem.

In the MAB formulation, the original POMDP problem is transformed into a number of smaller POMDPs distributed at the CCRs. These POMDPs are independent of each other, and each of them can be denoted as a tuple $\langle \check{\mathbb{S}}_z, \check{\mathbb{A}}_z, \check{\mathbf{P}}_z, \check{R}_z, \check{\mathbb{O}}_z, \check{\mathbf{Q}}_z \rangle$, where $\check{\mathbb{S}}_z$ is the state space, $\check{\mathbb{A}}_z$ is the action space, $\check{\mathbf{P}}_z$ is the state transition matrix, $\check{R}_z$ is the reward, $\check{\mathbb{O}}_z$ is the observation space, and $\check{\mathbf{Q}}_z$ is the observation probability matrix.

$$\begin{aligned} & P_s''^a(i,j) = P_s'^a(i,j)\eta(\dot{w}_i,\dot{w}_j) = \mathrm{P}(s''(t_{k+1}) = \dot{s}_j''|a(t_k) = \dot{a}_i, s''(t_k) = \dot{s}_i'') \\ = \; & \mathrm{P}\left(s'(t_{k+1}) = \dot{s}_j', w(t_{k+1}) = \dot{w}_j|a(t_k) = \dot{a}_i, s'(t_k) = \dot{s}_i', w(t_k) = \dot{w}_i\right) \mathrm{P}(w(t_{k+1}) = \dot{w}_j|w(t_k) = \dot{w}_i, a(t_k) = \dot{a}_i). \end{aligned} \tag{17}$$

Each element in the tuple is derived from the large augmented POMDP as follows.

$$\begin{aligned} \check{\mathbb{S}}_z &= \mathbb{S}_\beta \times \mathbb{H} \times \mathbb{W}_\delta \times \mathbb{W}^*_{\dot{\beta}_{z,j}}, \\ \check{\mathbb{A}}_z &= \{0,1\}, \\ \check{\mathbf{P}}_z &= \left[\check{P}_z^a(i,j)\right], \\ \check{R}_z &= R_z, \\ \check{\mathbb{O}}_z &= \mathbb{S}_\beta, \\ \check{\mathbf{Q}}_z &= \left[\mathrm{P}(o_z(t) = \dot{o}_{z,j}|\beta(z,t) = \dot{\beta}_i)\right] = \begin{bmatrix} \mathbf{I}_{S_\beta} \\ \mathbf{I}_{S_\beta} \end{bmatrix}. \end{aligned} \tag{18}$$

In (18), $\check{P}_z^a(i,j)$ is the element in the ith row and jth column of $\check{\mathbf{P}}_z$, and

$$\check{P}_z^a(i,j) = \check{P}_z''^a(i,j)\eta(\dot{w}_{z,i},\dot{w}_{z,j}), \tag{19}$$

where $\dot{w}_{z,i} \in \mathbb{W}_\delta \times \mathbb{W}^*_{\dot{\beta}_{z,j}}$ and $\dot{w}_{z,j} \in \mathbb{W}_\delta \times \mathbb{W}^*_{\dot{\beta}_{z,j}}$ are the realizations of the state $w_z(t)$, and $\check{P}_z''^a(i,j)$ is the ith row and jth column of $\check{\mathbf{P}}_z''$,

$$\check{\mathbf{P}}_z'' = \begin{bmatrix} \mathrm{P_H}(1,1)\mathbf{P}_z'^a & \mathrm{P_H}(1,2)\mathbf{P}_z'^a \\ \mathrm{P_H}(2,1)\mathbf{P}_z'^{\bar{a}} & \mathrm{P_H}(2,2)\mathbf{P}_z'^{\bar{a}} \end{bmatrix}. \tag{20}$$

Here, $\mathbf{P}_z'^a = \left[P_z'^a(i,j)\right]$, and

$$P_z'^a(i,j) = \begin{cases} 1, & \text{if } \dot{a}_z = 0 \text{ and } \dot{\beta}_{z,j} = \dot{\beta}_{z,i} \\ 0, & \text{if } \dot{a}_z = 0 \text{ and } \dot{\beta}_{z,j} \neq \dot{\beta}_{z,i} \\ P_z^a(i,j), & \text{if } \dot{a}_z = 1. \end{cases} \tag{21}$$

With this MAB formulation, a CCR z calculates its index $\psi(z,t)$ at time t according to its own augmented POMDP $\left\langle \check{\mathbb{S}}_z, \check{\mathbb{A}}_z, \check{\mathbf{P}}_z, \check{R}_z, \check{\mathbb{O}}_z, \check{\mathbf{Q}}_z \right\rangle$. Since the size of the POMDP at each CCR is much smaller, the computational complexity can be significantly reduce. Moreover, the SSP only needs to collect the indices $\psi(z,t), \forall z \in \mathbb{Z}$, and allocate the new band to the CCR with the largest $\psi(z,t)$ [33, 34].

VII. Optimal Spectrum Management

In this section, we describe the spectrum management mechanism, and analyze the sizes of the problems which directly determine the computational complexity.

A. Spectrum Management Process

In the network, the SSP makes the channel allocation decisions when new harvested bands are available for CaV packets. These bands are allocated to the CCRs with CaV packets one by one, and CCRs can utilize multiple bands simultaneously to transmit packets in a parallel manner. With the MAB formulation, the spectrum allocation is based on the indices of the CCRs, which are computed off-line and stored in local tables at the CCRs. In the on-line stage, a CCR only needs to lookup the table according to its current state and report the corresponding index to the SSP. The SSP simply selects the CCR with the largest index as the one to allocate a band.

Algorithm 1 On-line Harvested Band Allocation for CaV Packets at the SSP.

```
t ← 0;
σ ← FALSE;
while TRUE do
  establish a vector Υ = [ −∞ ... −∞ ], of which the length is Z;
  broadcast a message θ_R_Idx over the basic bands;
  update Υ(z) by ψ(z,t) when the message θ_Idx,z is received, until Υ[ 1 ... 1 ]^T ≠ −∞;
  while TRUE do
    if a message θ_ReV,z is received then
      if there are basic bands available then
        allocate a basic band to z and broadcast a message θ_Alloc,z to notify z;
      else
        σ ← TRUE;
      end if
    end if
    if a message θ_Init,z is received then
      break;
    end if
    if ℂ_t ≠ Φ then
      if σ == TRUE then
        allocate the first band in ℂ_t to z and broadcast a message θ_Alloc,z over the basic bands;
        σ ← FALSE;
      else
        z* ← argmax_{z∈ℤ} {Υ(z)};
        allocate the first band in ℂ_t to z* and broadcast a message θ_Alloc,z* over the basic bands;
        update Υ(z*) by ψ(z*,t) when the message θ_Idx,z* is received;
        broadcast a message θ_R_Idx over the basic bands;
      end if
    end if
  end while
  update t;
  update ℂ_t;
end while
```

The off-line computation is performed during network initialization. For each CCR z, the POMDP tuple $\left\langle \check{\mathbb{S}}_z, \check{\mathbb{A}}_z, \check{\mathbf{P}}_z, \check{R}_z, \check{\mathbb{O}}_z, \check{\mathbf{Q}}_z \right\rangle$ is input, and the finite set of indices $\left\{\psi_{z,\dot{\beta}_i}\right\}$ are off-line computed. Then, these indices are stored in a local table at each CCR with corresponding $\dot{\beta}_i$.

Algorithm 2 On-line Harvested Band Utilization for CaV Packets at the CCR z.

$t \leftarrow 0$;
$\sigma_z \leftarrow$ TRUE;
while TRUE **do**
  if an ReV packet arrives at z for transmitting **then**
    send a message $\theta_{\text{ReV},z}$ to the SSP;
    put the ReV packet in the transmission queue before all CaV packets;
  end if
  if a CaV packet arrives at z for transmitting and $\sigma ==$ FALSE **then**
    send a message $\theta_{\text{Init},z}$ to the SSP;
    $\sigma_z \leftarrow$ TRUE;
  end if
  if a message $\theta_{\text{R\_Idx}}$ or $\theta_{\text{Alloc},z}$ is received **then**
    update $\beta(z,t)$;
    lookup the local index table to determine $\psi(z,t)$;
    send a message $\theta_{\text{Idx},z}$ incorporating $\psi(z,t)$ to the SSP;
    $\sigma_z \leftarrow$ TRUE;
  end if
  if a message $\theta_{\text{Alloc},z}$ is received **then**
    utilize the allocated band to transmit the first packet in z's transmission queue;
  end if
  if a message $\theta_{\text{Alloc},z'}$ is received, $z \neq z'$, and the transmission queue length is 0 **then**
    $\sigma_z \leftarrow$ FALSE;
  end if
  update t;
end while

The on-line allocation process operated at the SSP to make band allocation decision for CaV packets is described in Algorithm 1. The on-line operation of a CCR z is presented in Algorithm 2. In these algorithms, σ is the indicator to denote whether an ReV packet is waiting for the harvested band, σ_z is the indicator to denote whether the state of z changes when $a(t) \neq z$, and $\bullet^{\mathrm{T}}$ denotes the transpose operation of a vector. Several messages are defined as follows.

$\theta_{\text{ReV},z}$: The unicast message from the CCR z to the SSP to notify an ReV packet in z's queue.

$\theta_{\text{Idx},z}$: The unicast message from the CCR z to the SSP to notify the current index $\psi(z,t)$ of z.

$\theta_{\text{Init},z}$: The unicast message from the CCR z to the SSP to request for re-starting the allocation process.

$\theta_{\text{R\_Idx}}$: The broadcast message from the SSP to all the CCRs to request their current indices.

$\theta_{\text{Alloc},z}$: The broadcast message from the SSP to all the CCRs to notify the allocation decision.

$\theta_{\text{Stop},z,c}$: The unicast message from the SSP to the CCR z to require immediate stop of transmission over the band c.

B. Size of the POMDP Problem

The computational complexity for solving a POMDP problem depends on the sizes of the state space, action space and observation space. In the augmented POMDP formulation, the size of the action space $|\mathbb{A}''| = Z$, and the size of the observation space $|\mathbb{O}''| = S = {S_\beta}^Z$. The state space $\mathbb{S}'' = \mathbb{S} \times \mathbb{H} \times \mathbb{W}_\delta \times \left(\mathbb{W}^*_{\dot{\beta}_{z,j}}\right)^Z$, of which the size is

$$S'' = S\,|\mathbb{H}|\,W_\delta \left(W^*_{\dot{\beta}_{z,j}}\right)^Z = 2W_\delta \left(S_\beta W^*_{\dot{\beta}_{z,j}}\right)^Z. \quad (22)$$

Note that $\mathbb{W}^*_{\dot{\beta}_{z,j}}$ is the state space of $\hat{P}^*_{\dot{\beta}_{z,j}}$ for all $\dot{\beta}_{z,j} \in \mathbb{S}_\beta$ and $\dot{\beta}_{z,j} \neq \dot{\beta}_0$. Thus, $W^*_{\dot{\beta}_{z,j}} = W_\beta^{S_\beta - 1}$, where W_β denotes the size of the state space of one $\hat{P}^*_{\dot{\beta}_{z,j}}$. As S_β grows, $W^*_{\dot{\beta}_{z,j}}$ can be very large. However, we can significantly reduce the size of $\mathbb{W}^*_{\dot{\beta}_{z,j}}$ based on the constraint that $\sum_{\forall \dot{\beta}_{z,j} \in \mathbb{S}_\beta, \dot{\beta}_{z,j} \neq \dot{\beta}_0} P^*_{\dot{\beta}_{z,j}} = 1$. Suppose that we transform the continuous $P^*_{\dot{\beta}_{z,j}}$ to discrete $\hat{P}^*_{\dot{\beta}_{z,j}}$ as

$$\hat{P}^*_{\dot{\beta}_{z,j}} = \frac{m}{W_\beta - 1}, \text{if } \frac{2m-1}{2W_\beta - 2} \leq P^*_{\dot{\beta}_{z,j}} < \frac{2m+1}{2W_\beta - 2}, \quad (23)$$

where $0 \leq m \leq W_\beta - 1$. Then, to derive the value of $W^*_{\dot{\beta}_{z,j}}$, we first introduce a lemma as follows.

Lemma 3. *Let $\zeta(n)$ represent a random variable that $\frac{2n-1}{2W_\beta - 2} \leq \zeta(n) < \frac{2n+1}{2W_\beta - 2}$, where n is an integer satisfying $0 \leq n \leq 2W_\beta - 1$. A set $\{n_1, \ldots, n_k, \ldots, n_K\}$ is called the base set of the set $\{\zeta(n_1), \ldots, \zeta(n_k), \ldots \zeta(n_K)\}$. Let $N(m,K)$ denote the number of sets $\{n_1, \ldots, n_k, \ldots, n_K\}$ that satisfy $\frac{2m-1}{2W_\beta - 2} \leq \sum_{k=1}^K \zeta(n_k) < \frac{2m+1}{2W_\beta - 2}$. Then, $N(m,K)$ satisfies inequality (24).*

Proof. Available in Section 4 in our proofs of the lemmas and theorems [29]. □

According to Eqn. (8), if $S_\beta = 1$, the only possible realization of $\beta(z,t)$ is $\dot{\beta}_0$. If $S_\beta = 2$, the only possible realization of $\beta(z,t)$ other than $\dot{\beta}_0$ must have $P^*_{\dot{\beta}_{z,j}} = 1$. When $S_\beta \geq 3$, the bound of $W^*_{\dot{\beta}_{z,j}}$ is given by the theorem as follows.

Theorem 2. *If $S_\beta \geq 3$, $W^*_{\dot{\beta}_{z,j}}$ satisfies inequality (25).*

Proof. Available in Section 5 in our proofs of the lemmas and theorems [29]. □

With Theorem 2 and Eqn. (22), the upper and lower bounds of the state space size S'' can be calculated.

C. Size of the MAB Problem

In the MAB formulation, the size of the action space $\left|\check{\mathbb{A}}\right| = 2$, the size of the observation space $\left|\check{\mathbb{O}}\right| = S_\beta$, and the size of the state space can be calculated as

$$\check{S}_z = S_\beta\,|\mathbb{H}|\,W_\delta W^*_{\dot{\beta}_{z,j}} = 2S_\beta W_\delta W^*_{\dot{\beta}_{z,j}}. \quad (26)$$

These parameters in the MAB formulation are much smaller than those in the POMDP formulation. Therefore, the computational complexity can be significantly reduced by the MAB formulation. We will further evaluate the complexity performance in Section VIII.

$$\binom{m'+K-1}{K-1} \leq N(m,K) \leq \sum_{m'=(\lfloor 2m-K+1/2 \rfloor)^+}^{\lceil 2m+K+1/2 \rceil} \binom{m'+K-1}{K-1}. \tag{24}$$

$$\sum_{m=0}^{W_\beta-1} \binom{m+S_\beta-3}{S_\beta-3} \leq W^*_{\dot{\beta}_{z,j}} \leq \sum_{m=0}^{W_\beta-1} \sum_{m'=\lfloor 2m-S_\beta+3/2 \rfloor}^{\lceil 2m+S_\beta-1/2 \rceil} \binom{m'+S_\beta-3}{S_\beta-3}. \tag{25}$$

VIII. Simulation Results and Analysis

Extensive simulation results are presented in this section to demonstrate the performance of the proposed scheme. In our simulations, 30 CCRs and 300 users are randomly distributed in the network. Each user connects to its nearest CCR to receive video streaming services. Orthogonal frequency division multiplexing (OFDM) is adopted as the physical layer technology for wireless communications over Rayleigh fading channels among CCRs and users. We set the average data rate of the link between two CCRs as $\bar{\omega}_y = 25$ Mbps, The harvesting rates $\lambda_{\text{H},1}$ and $\lambda_{\text{H},2}$ of harvested bands during busy time and idle time are 0.01 and 0.04, respectively, and the expected portions of busy time and idle time are 40% and 60%, respectively. The arrival rate λ_z of CaV packets at each CCR is 0.4, and the video streaming bit rate for highest quality ω_{max} is 14 Mbps, with the video sequences Bus, Foreman, Mobile and Coastguard at 30 frames per second. Both PSNR and distortion (i.e., mean square error, MSE) performances of the video are presented in the simulations as the average values over the four video sequences. We set $P_\delta = 0.02$. Besides, 5 levels are used to obtain the discrete random variables, i.e., $W_\delta = W^*_{\dot{\beta}_{z,j}} = S_\beta = 5$.

In our simulations, we compare five different schemes: The no-caching scheme that delivers video traffic in secondary networks without caching; the passive scheme that caches only on-route data and can be considered as the scheme without cognitive radio capability as shown in [28]; the proactive scheme that proactively caches the data without considering resource allocation, similar to what is discussed in [9]; the greedy scheme that allocates the harvested bands to the links with the highest $\tilde{\beta}(z,t)$; and the proposed optimal scheme that allocates the harvested bands according to the index $\psi(z,t)$ in our formulation.

A. Video Quality Performance

We first compare the PSNR of video streaming with different schemes in Fig. 2a, 2b and 2c with different parameters. In Fig. 2a, the average PSNR of the optimal, greedy, proactive, passive and no-caching schemes is shown with varying network size. We can see that as the number of CCRs grows, the average PSNR decreases for all the five schemes considered, because larger network size will result in higher delay and lower bit rate for the video contents that are not cached at CCRs close to the users. When the passive scheme is used, video segments are only cached at the on-route CCRs, and thus the average PSNR is drastically degraded with the increase of network size. Differently, proactive caching allows video segments to be pushed to the CCRs close to the users with possible future interests. Therefore, proactive, greedy and optimal schemes all perform better than the passive one. The performance of the no-caching scheme is even worse. It can be observed that the optimal scheme achieves up to 2.5 dB PSNR improvement compared to the passive scheme.

The capacity of the wireless links in the network also has significant effect on the PSNR performance as shown in Fig. 2b. Note that here we use mean link capacity in the figure to describe the quality of Rayleigh fading wireless channels considered in the simulations, which represents the expected data rate from one CCR to its directly-connected CCR or user. We can observe that as the link capacity between the CCRs increases, the average PSNR increases as well, and our proposed optimal spectrum management scheme significantly outperforms the other schemes.

We also compare the PSNR performance with different video source coding rate ω_{max} in Fig. 2c. Here, ω_{max} represents the source coding bit rate of the original video file. Thus, any video transmission rate higher than ω_{max} would not contribute to the PSNR. In Fig. 2c, we can observe that PSNR increases with the video source coding rate when $\omega_{\text{max}} \leq 8$ Mbps. However, it does not increase any more when $\omega_{\text{max}} > 8$ Mbps, because of the throughput limitation of the path from the video streaming servers/caching CCRs to the users. Moreover, our proposed scheme always provides much higher PSNR compared to the other schemes.

In Fig. 3a, 3b and 3c, the video distortion measured in MSE is compared among the five schemes. Similar conclusions can be drawn and the proposed scheme always outperforms the other ones.

B. Transmission Delay Performance

Transmission delay is another key performance metric for video streaming in IC-CRNs. Users may give up watching the video because of the long waiting time for video buffering. In this subsection, we evaluate the average transmission delay performance and the results are shown in Fig. 4a, 4b and 4c.

In Fig. 4a, we can observe that a larger number of CCRs in the IC-CRN result in higher average delay due to the longer transmission path. The average packet delay with the proactive scheme is slightly smaller compared to the passive scheme, but the greedy scheme induces larger delay in an IC-CRN when the number of the CCRs is more than 30. This is because the greedy scheme selects the CCR with the largest continuous state $\tilde{\beta}(z,t)$, which is defined to be inversely proportional to the number of hops $\xi(\pi)$ from the

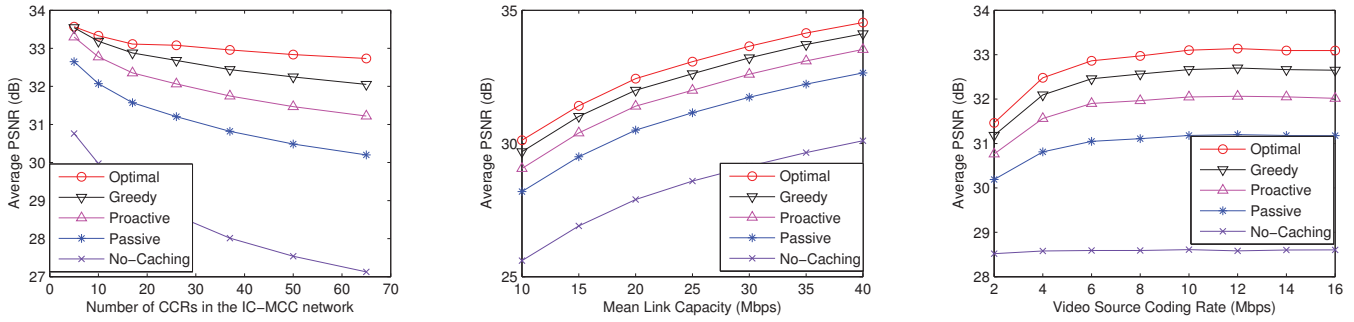

(a) (b) (c)

Fig. 2: Average PSNR of the video streaming with different (a) number of CCRs in the IC-CRN, (b) maximum link capacity, and (c) video source coding rate.

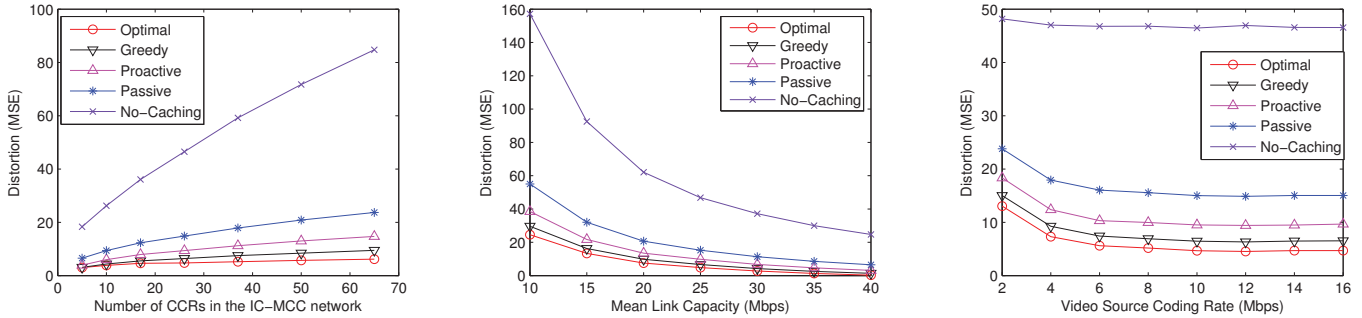

(a) (b) (c)

Fig. 3: Average video distortion (MSE) of the video streaming with different (a) number of CCRs in the IC-CRN, (b) maximum link capacity, and (c) video source coding rate.

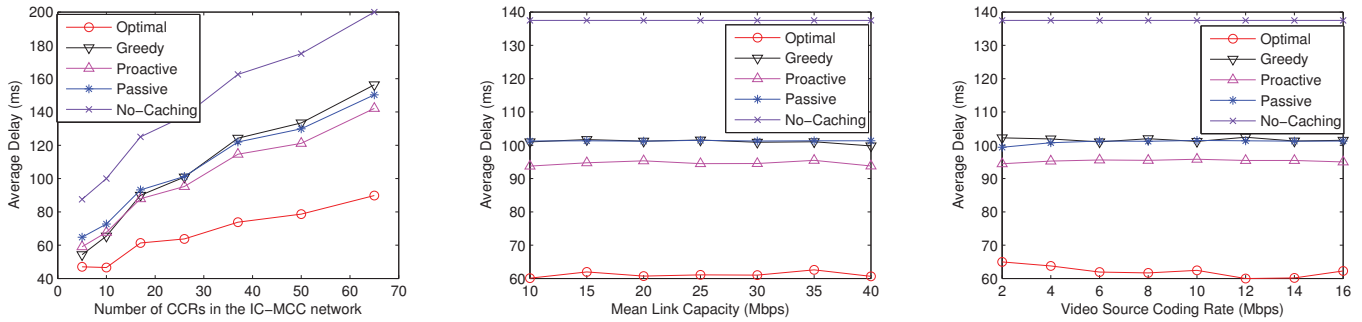

(a) (b) (c)

Fig. 4: Average packet delay with different (a) number of CCRs in the IC-CRN, (b) maximum link capacity, and (c) video source coding rate.

video server to the destination CCR. Thus, it tends to select the CCRs with lower $\xi(\pi)$, which improves the hit ratio and video quality while sacrificing the packet delay performance. Different from the greedy scheme, our proposed optimal scheme can improve the video quality and the packet delay performance simultaneously.

From Fig. 4b and 4c, we can observe that the packet delay performance of the five schemes does not change much with mean link capacity and video source coding rate. Our proposed optimal spectrum management scheme reduces the average delay by about 40%.

C. Hit Ratio Performance

The hit ratio is widely adopted as the performance metric to evaluate the caching mechanisms used in ICNs. Since ICN is not considered in the no-caching scheme, the hit ratio is always zero. Consequently, we omit the no-caching scheme in this subsection and illustrate the average hit ratio of the cached contents of the other four schemes in our simulations in Fig. 5a, 5b and 5c. Due to the optimal spectrum management and proactive caching operations, the proposed scheme improves the average hit ratio performance by around 60% compared to the passive caching scheme, when $5 \leq Z \leq 65$, 2 Mbps

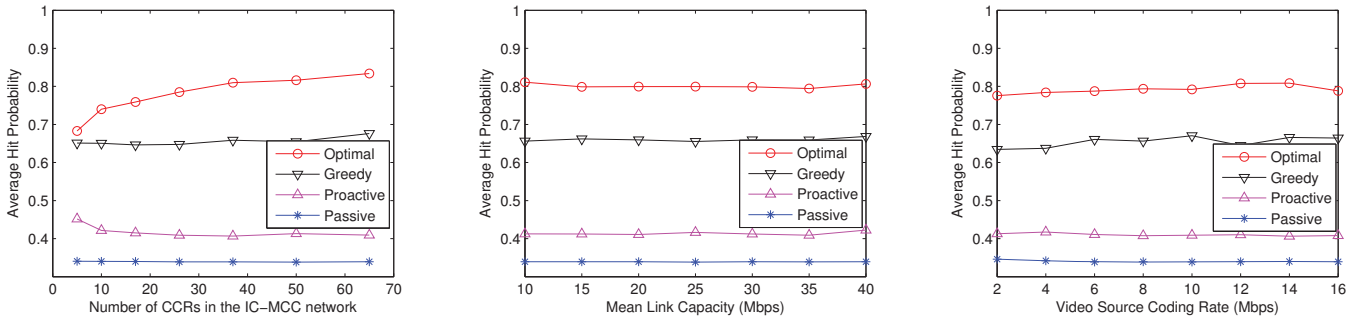

Fig. 5: Average hit ratio with different (a) number of CCRs in the IC-CRN, (b) maximum link capacity, and (c) video source coding rate.

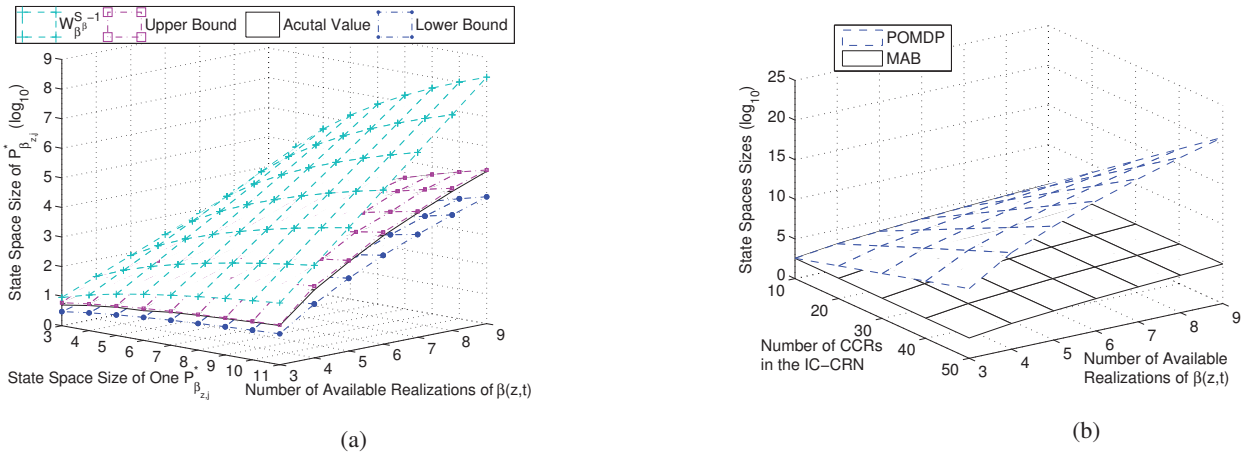

Fig. 6: State space size (a) of $\hat{P}^*_{\dot{\beta}_{z,j}}$, and (b) with different number of available realizations of $\beta(z,t)$.

$\leq \omega_{\max} \leq 40$ Mbps, and mean link capacity from 10 Mbps to 40 Mbps.

D. Problem Size

We also study the problem sizes by simulations, of which the results are shown in Fig. 6a and 6b. In Section VII-B, we show that the size of $\mathbb{W}^*_{\dot{\beta}_{z,j}}$ can be reduced from $W_\beta^{S_\beta-1}$ to a much smaller value $W^*_{\dot{\beta}_{z,j}}$. However, the value of $W^*_{\dot{\beta}_{z,j}}$ is hard to be theoretically derived. So we find out its upper and lower bounds in Theorem 2. Here, the actual value of $W^*_{\dot{\beta}_{z,j}}$ obtained by simulations, the upper and lower bound of $W^*_{\dot{\beta}_{z,j}}$, and $W_\beta^{S_\beta-1}$ are shown in Fig. 6a. We can observe that the bounds are very tight, and $W^*_{\dot{\beta}_{z,j}} \ll W_\beta^{S_\beta-1}$.

Furthermore, in Fig. 6b, the problem sizes of the POMDP and MAB formulation are compared. We can observe that the size of the POMDP formulation is much larger than that of the MAB formulation. The MAB problem size grows with the number of available realizations of $\beta_{z,t}$, but it does not depend on the number of CCRs Z. This is because each CCR only needs to find out its own index according to its own state. Thus, the MAB formulation is scalable.

In a typical setting with $W_\beta = W_\delta = S_\beta = 5$, the state space size of the MAB formulation $\check{S}_Z = 14800$, the action space size $\left|\check{\mathbb{A}}\right| = 2$ and the observation space size $\left|\check{\mathbb{O}}\right| = 5$. We can use reasonable time to solve such an MAB problem with the recent advanced POMDP algorithms [35–37]. For example, 1924 seconds in the off-line calculation stage and less than 10 milliseconds in the on-line decision making stage are taken to solve it on our computer with Intel® Core™i5-4300U 2.50GHz CPU and 4 GB RAM. Although the off-line calculation is time-consuming, the network performance will not degrade, since the off-line calculation needs to be run only once during the network initialization.

IX. Conclusions

In this paper, a new architecture of IC-CRN has been introduced to support wireless video streaming while efficiently utilizing the harvested bands for delay-tolerant proactive caching video traffic. We also proposed a dynamic spectrum management scheme for optimal video PSNR, and formulated it as an HDP-MDP, taking into account the unknown/changing network parameters and queueing states at the CCRs. We then reformulated it as a POMDP and an MAB problem for optimal spectrum allocation scheme. We further discussed the band allocation mechanism and analyzed the problem sizes. Extensive simulation results were also provided to demonstrate

the significant performance improvement of our proposed scheme comparing to the existing ones.

As our future work, we will build the real system and conduct subjective video quality tests to evaluate the performance of the proposed scheme.

ACKNOWLEDGMENT

The authors would like to thank the anonymous reviewers for their comments and suggestions to improve the paper.

REFERENCES

[1] T. Koponen, M. Chawla, B.-G. Chun, A. Ermolinskiy, K. H. Kim, S. Shenker, and I. Stoica, "A data-oriented (and beyond) network architecture," *ACM SIGCOMM Computer Communication Review*, vol. 37, no. 4, pp. 181–192, 2007.

[2] N. Fotiou, D. Trossen, and G. C. Polyzos, "Illustrating a publish-subscribe internet architecture," *Telecommunication Systems*, vol. 51, no. 4, pp. 233–245, 2012.

[3] K. Pentikousis, "Distributed information object resolution," in *Proc. the 8th International Conference on Networks (ICN)*, (Gosier, France), pp. 360–366, Mar. 2009.

[4] V. Jacobson, D. K. Smetters, J. D. Thornton, M. F. Plass, N. H. Briggs, and R. L. Braynard, "Networking named content," in *Proc. the 5th International Conference on Emerging Networking Experiments and Technologies*, (Rome, Italy), pp. 1–12, Dec. 2009.

[5] D. Trossen and G. Parisis, "Designing and realizing an information-centric Internet," *IEEE Communications Magazine*, vol. 50, no. 7, pp. 60–67, 2012.

[6] G. Xylomenos, C. N. Ververidis, V. A. Siris, N. Fotiou, C. Tsilopoulos, X. Vasilakos, K. V. Katsaros, and G. C. Polyzos, "A survey of information-centric networking research," *IEEE Communications Surveys & Tutorials*, vol. 16, no. 2, pp. 1024–1049, 2014.

[7] X. Wang, M. Chen, T. Taleb, A. Ksentini, and V. C. M. Leung, "Cache in the air: exploiting content caching and delivery techniques for 5G systems," *IEEE Communications Magazine*, vol. 52, no. 2, p. 132, 2014.

[8] J. Mitola and G. Q. Maguire Jr, "Cognitive radio: making software radios more personal," *IEEE Personal Communications*, vol. 6, no. 4, pp. 13–18, 1999.

[9] Y.-T. Yu, C. Tandiono, X. Li, Y. Lu, M. Sanadidi, and M. Gerla, "ICAN: information-centric context-aware ad-hoc network," in *Proc. 2014 International Conference on Computing, Networking and Communications (ICNC)*, (Honolulu, Hawaii), Feb. 2014.

[10] H. Ko, Y. Kim, D. Suh, and S. Pack, "A proactive content pushing scheme for provider mobility support in information centric networks," in *Proc. the 11th IEEE Consumer Communications and Networking Conference (CCNC)*, (Las Vegas, NV), pp. 523–524, Jan. 2014.

[11] S. Jung, H. Park, T. Woo, and T. Kwon, "Data pushing using IPT in content-centric networking," in *Proc. the 6th International Conf on Ubiquitous and Future Networks (ICUFN)*, (Shanghai, China), pp. 164–165, July 2014.

[12] C. Tsilopoulos, D. Makris, and G. Xylomenos, "Bootstrapping a publish/subscribe information centric network," in *Proc. 2011 Future Network & Mobile Summit (FutureNetw)*, (Warsaw, Poland), June 2011.

[13] Y. Zhu and A. Nakao, "A deployable and scalable information-centric network architecture," in *Proc. 2013 IEEE International Conference on Communications (ICC)*, (Budapest, Hungary), pp. 3753–3758, June 2013.

[14] L. Han, S.-S. Kang, H. Kim, and H. P. In, "Adaptive retransmission scheme for video streaming over content-centric wireless networks," *IEEE Communications Letters*, vol. 17, no. 6, pp. 1292–1295, 2013.

[15] B. Han, X. Wang, N. Choi, T. Kwon, and Y. Choi, "AMVS-NDN: Adaptive mobile video streaming and sharing in wireless named data networking," in *Proc. 2013 IEEE Conference on Computer Communications Workshops (INFOCOM WKSHPS)*, (Turin, Italy), pp. 375–380, Apr. 2013.

[16] Y. Liu, J. Geurts, J.-C. Point, S. Lederer, B. Rainer, C. Muller, C. Timmerer, and H. Hellwagner, "Dynamic adaptive streaming over CCN: a caching and overhead analysis," in *Proc. 2013 IEEE International Conference on Communications (ICC)*, (Budapest, Hungary), pp. 3629–3633, June 2013.

[17] R. Grandl, K. Su, and C. Westphal, "On the interaction of adaptive video streaming with content-centric networking," in *Proc. 20th International Packet Video Workshop (PV)*, (San Jose, CA), Dec. 2013.

[18] C. Tsilopoulos, G. Xylomenos, and G. C. Polyzos, "Are information-centric networks video-ready?," in *Proc. 20th International Packet Video Workshop (PV)*, (San Jose, CA), Dec. 2013.

[19] J. Zhao, W. Gao, Y. Wang, and G. Cao, "Delay-constrained caching in cognitive radio networks," *IEEE Transactions on Mobile Computing*, online published, 2015.

[20] ICN Research Group, "icnrg – IRTF," http://trac.tools.ietf.org/group/irtf/trac/wiki/icnrg, 2015.

[21] R. A. Rehman, J. Kim, and B.-S. Kim, "NDN-CRAHNs: Named data networking for cognitive radio ad hoc networks," *Mobile Information Systems*, vol. 2015, accepted for publication, 2015.

[22] M. Pan, C. Zhang, P. Li, and Y. Fang, "Spectrum harvesting and sharing in multi-hop CRNs under uncertain spectrum supply," *IEEE Journal on Selected Areas in Communications*, vol. 30, no. 2, pp. 369–378, 2012.

[23] H. Yue, M. Pan, Y. Fang, and S. Glisic, "Spectrum and energy efficient relay station placement in cognitive radio networks," *IEEE Journal on Selected Areas in Communications*, vol. 31, no. 5, pp. 883–893, 2013.

[24] M. Li, P. Li, X. Huang, Y. Fang, and S. Glisic, "Energy consumption optimization for multihop cognitive cellular networks," *IEEE Transactions on Mobile Computing*, vol. 14, no. 2, pp. 358–372, 2015.

[25] R. Ahmed, M. F. Bari, S. R. Chowdhury, M. G. Rabbani, R. Boutaba, and B. Mathieu, "αRoute: A name based routing scheme for information centric networks," in *Proc. 2013 IEEE International Conference on Computer*

Communications (INFOCOM), (Turin, Italy), Apr. 2013.

[26] S. Ma, W. Gao, and Y. Lu, "Rate-distortion analysis for H.264/AVC video coding and its application to rate control," *IEEE Transactions on Circuits and Systems for Video Technology*, vol. 15, no. 12, pp. 1533–1544, 2005.

[27] X. Zhao, J. Sun, S. Ma, and W. Gao, "Novel statistical modeling, analysis and implementation of rate-distortion estimation for H. 264/AVC coders," *IEEE Transactions on Circuits and Systems for Video Technology*, vol. 20, no. 5, pp. 647–660, 2010.

[28] I. Psaras, W. K. Chai, and G. Pavlou, "In-network cache management and resource allocation for information-centric networks," *IEEE Transactions on Parallel and Distributed Systems*, vol. 25, no. 11, pp. 2920–2931, 2014.

[29] P. Si, H. Yue, Y. Zhang, and Y. Fang, "Proofs of the lemmas and theorems in "spectrum management for proactive video caching in information-centric cognitive radio networks"," Internet: http://sipengbo.wikispaces.com/file/view/Proofs.pdf/, May 26, 2015, [May 28, 2015].

[30] S. P. Choi, N. L. Zhang, and D.-Y. Yeung, "Solving hidden-mode Markov decision problems," in *Proc. the 8th International Workshop on Artificial Intelligence and Statistics*, (Key West, Florida), Jan. 2001.

[31] H. Bai, D. Hsu, and W. S. Lee, "Planning how to learn," in *Proc. 2013 IEEE International Conference on Robotics and Automation (ICRA)*, (Karlsruhe, Germany), May 2013.

[32] C. H. Papadimitriou and J. N. Tsitsiklis, "The complexity of Markov decision processes," *Mathematics of operations research*, vol. 12, no. 3, pp. 441–450, 1987.

[33] J. Gittins, K. Glazebrook, and R. Weber, *Multi-armed bandit allocation indices*. John Wiley & Sons, 2011.

[34] P. Whittle, "Multi-armed bandits and the Gittins index," *Journal of the Royal Statistical Society. Series B (Methodological)*, pp. 143–149, 1980.

[35] S. Paquet, B. Chaib-draa, and S. Ross, "Hybrid POMDP algorithms," in *Proc. Workshop on Multi-Agent Sequential Decision Making in Uncertain Domains (MSDM)*, (Hakodate, Japan), pp. 133–147, May 2006.

[36] T. Smith and R. Simmons, "Heuristic search value iteration for POMDPs," in *Proc. the 20th conference on Uncertainty in Artificial Intelligence*, (Banff, Canada), pp. 520–527, July 2004.

[37] S. Paquet, L. Tobin, and B. Chaib-Draa, "An online POMDP algorithm for complex multiagent environments," in *Proc. the 4th International Joint Conference on Autonomous Agents and Multiagent Systems*, (Utrecht, Netherlands), pp. 970–977, July 2005.

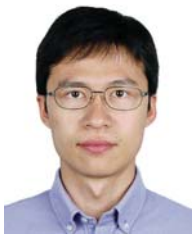

Pengbo Si (SM'15) received the B.E. and Ph.D. degrees in communications engineering and communication and information system both from Beijing University of Posts and Telecommunications, Beijing, China, in 2004 and 2009, respectively. He joined Beijing University of Technology, Beijing, China, in 2009, where he is currently an Associate Professor. From 2007 to 2008, he was a Visiting Ph.D. Student at Carleton University, Ottawa, Canada. From 2014 to 2015, he was a Visiting Scholar at University of Florida, Gainesville, FL, USA. Dr. Si received the Best Paper Runner Up Award from the 2015 International Conference on Wireless Algorithms, Systems, and Applications. He serves as the Associate Editor of International Journal on AdHoc Networking Systems, the Editorial Board Member of Ad Hoc & Sensor Wireless Networks, and the Guest Editor of Advances in Mobile Cloud Computing, IEEE Transactions on Emerging Topics in Computing Special Issue. He also served as the TPC Co-Chair of the IEEE ICCC-GMCN'2013, Program Vice-Chair of IEEE GreenCom'2013. He is a Senior Member of the IEEE.

Hao Yue (M'15) received his B.S. degree in Telecommunication Engineering from Xidian University, Xi'an, China, in 2009, and Ph.D. degree in Electrical and Computer Engineering from University of Florida, Gainesville, FL, USA, in 2015. He is now an Assistant Processor with the Department of Computer Science, San Francisco State University, San Francisco, CA, USA. His research interests include cyber-physical systems, cybersecurity, wireless networking, and mobile computing.

Yanhua Zhang received the B.E. degree from Xi'an University of Technology, Xi'an, China, in 1982, and the M.S. degree from Lanzhou University, Lanzhou, China, in 1988. From 1982 to 1990, he was with Jiuquan Satellite Launch Center (JSLC), Jiuquan, China. During the 1990s, he was a visiting professor at Concordia University, Montreal, Canada. He joined Beijing University of Technology, Beijing, China, in 1997, where he is currently a professor.

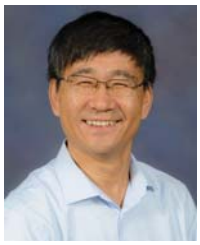

Yuguang Fang (F'08) received an MS degree from Qufu Normal University, Shandong, China in 1987, a Ph.D degree from Case Western Reserve University in 1994 and a Ph.D. degree from Boston University in 1997. He joined the Department of Electrical and Computer Engineering at University of Florida in 2000 and has been a full professor since 2005. He holds a University of Florida Research Foundation (UFRF) Professorship from 2006 to 2009, a Changjiang Scholar Chair Professorship with Xidian University, China, from 2008 to 2011, and a Guest Chair Professorship with Tsinghua University, China, from 2009 to 2012. Dr. Fang received the US National Science Foundation Career Award in 2001, the Office of Naval Research Young Investigator Award in 2002, the 2010-2011 UF Doctoral Dissertation Advisor/Mentoring Award, the 2011 Florida Blue Key/UF Homecoming Distinguished Faculty Award, and the 2009 UF College of Engineering Faculty Mentoring Award. He is the Editor-in-Chief of IEEE Transactions on Vehicular Technology, was the Editor-in-Chief of IEEE Wireless Communications (2009-2012) and serves/served on several editorial boards of journals including IEEE Transactions on Mobile Computing, IEEE Transactions on Communications and IEEE Transactions on Wireless Communications. He has been actively participating in conference organizations such as serving as the Technical Program Co-Chair for IEEE INOFOCOM'2014. He is a fellow of the IEEE and the AAAS.